Effect of Subgrade on Tensile Strains in a Geomembrane for Tailings Storage Applications

Jiying Fan and R. Kerry Rowe*

Jiying Fan. Postdoctoral Fellow, GeoEngineering Centre at Queen's-RMC, Dept. of Civil Engineering, Queen's Univ., Kingston, ON, Canada K7L 3N6, ORCID: 0000-0002-4632-1980. Email: jiying.fan@queensu.ca

R. Kerry Rowe. Barrington Batchelor Distinguished University Professor, Canada Research Chair in Geotechnical and Geoenvironmental Engineering, GeoEngineering Centre at Queen's-RMC, Dept. of Civil Engineering, Queen's Univ., Kingston, ON, Canada K7L 3N6, ORCID: 0000-0002-1009-0447. Email: kerry.rowe@queensu.ca

*Corresponding author

Abstract: Experiments are conducted to quantify short-term tensile strains induced in a 1.5-mm-thick high-density polyethylene geomembrane overlain by tailings. Four subgrades, a poorly graded angular to sub-angular gravel (GP), a well-graded angular to sub-angular gravel (GW), a poorly subrounded graded sand (SP), and silty sand (SM), and two nonwoven geotextiles, 450 g/m^2 and 1420 g/m^2, are evaluated. All the indentations in the geomembrane are due to the subgrade, and with an adequate fraction of sand size particles in the subgrade, the tensile strains can be minimized. At 2000 kPa, the maximum tensile strain is 32% for GP, 16% for GW, 13% for SP, and no discernable indentation is observed for SM prepared at the optimum water content of 11%. For the soft SM subgrade prepared at 20% water content, only one indentation with the tensile strain of 2% is observed. At 2000 kPa, a 450 g/m^2 geotextile beneath the GMB reduces the maximum tensile strain from 32% to 23% for GP subgrade, from 16% to 8% for GW subgrade, and from 13% to 6% for SP subgrade; the 1420 g/m^2 geotextile reduces the maximum tensile strain to 14% for GP subgrade. Thus, minimal subgrade indentation induced strain and hence the possibility of a very long service life of geomembrane can be achieved using SM subgrade.

Keywords: Geosynthetics, Geomembrane, Geotextile, Tailings, Geomembrane Strain

1. Introduction

Tailings storage facilities (TSFs) are engineered structures constructed to impound slurry, thickened, and paste tailings resulting from mineral processing activities. With the increase in the footprint of mining sites and the height of tailing dams, geomembranes (GMBs) are increasingly playing a vital role in the containment and erosion control of these facilities (Davies et al. 2002; Thiel and Smith 2004; Touze et al. 2008; Touze 2020; Rowe 2020).

The GMB in mining applications is usually either high-density polyethylene (HDPE) or linear low-density polyethylene (LLDPE) with a typical thickness of 1.0 to 2.5 mm (Touze et al. 2008; Rowe et al. 2013). To the extent that these GMBs have been used in TSFs, it has most commonly been either as a liner to the tailings dam wall (Giroud 2016; McLeod 2016) or a GMB liner placed on the base in order to reduce the contaminant migration, leakage, and the hydraulic gradient from the facilities to the surrounding environment, and decrease the phreatic surface within the embankment dam to achieve adequate geotechnical stability against failure (Lupo and Morrison 2007; Touze et al. 2008; Rowe et al. 2017; Chou et al. 2018; Rowe 2020; Fan and Rowe 2022a, 2022b; Rowe and Fan 2021, 2022). GMB liner systems for TSFs commonly comprise a single GMB liner even though the hydraulic head within the facility can exceed 100 m (Touze et al. 2008). This is because tailings with a typical fines content (<75 μm) of 40-70% can form a lower permeability layer at the base of TSFs above the liner. With these GMBs, the leakage is effectively limited to flow through holes in the GMB that most arise either from short-term puncture (e.g., during construction including placement of materials over the GMB) or subsequently due to long-term stress cracking (Giroud and Bonaparte 1989a, 1989b; Giroud 1997; Peggs et al. 2005, 2014; Rowe 1998, 2005, 2012, 2020; Rowe and Yu 2019; Abdelaal et al. 2014; Ewais et al., 2014).

Given the large size and remote location of TSFs, the subgrade soil beneath the GMB is often the in-situ or recompacted soil or rock. Therefore, the GMB may be subject to indentions that indue tensile strain from this subgrade. Current practice to assess the performance of GMB with proposed materials overlying and underlying is to conduct short-term cylinder test for 24-100 h to examine whether the GMB punctures (Thiel and Smith 2004; Lupo and Morrison 2007; Brachman at al. 2014). While it is necessary to avoid short-term puncture, the absence of puncture does not mean that holes will not develop with time in areas where there are high tensile strains due to stress cracking. Indentations may arise from stones in the subgrade below the GMB (Brachman and Sabir 2010) or a drainage layer below waste, crushed ore, or tailings (e.g., Rowe et al. 2013; Brachman et al. 2014; Marcotte and Fleming 2019, 2020; Rowe and Yu 2019; Rowe 2020). These indentations induced tensile strain have ben shown to cause stress cracking at strains as low as 5% (Abdelaal et al. 2014; Ewais et al. 2014). Thus, there may also be a need to limit the local tensile strains in the GMB that develop at indentations from overlying or underlying materials to ensure adequate long-term performance (Seeger and Müller 2003; Hornsey and Wishaw 2012; Eldesouky and Brachman 2020). Although much is known about local tensile strains that may develop in a municipal solid waste landfill and heap leach applications primarily from gravel above the liner (Tognon et al. 2000; Brachman and Gudina 2008; Rowe et al. 2013; Brachman et al. 2014; Marcotte and Fleming 2019, 2020; Adesokan et al. 2021), there is a paucity of data on the tensile strains that may develop from the subgrade below the GMB in tailings storage facilities.

The magnitude of allowable tensile strains that a GMB can sustain without compromising their intended long-term performance reported in the literature varies (Seeger and Müller 2003; Peggs et al. 2005; Rowe et al. 2019b). For example, to avoid premature GMB failure due to stress cracking, Seeger and Müller (2003) recommended that the GMB strain should be less than 3%. Coming from a different perspective, Rowe et al. (2019b) suggested 3-5% depending on the location of the GMB (i.e., 3% on the base, 4% on side slopes, 5% on in the cover). Based on the GMBs examined under the simulated field conditions, it can be inferred that the tensile strains due to a granular drainage layer in a leachate collections system, below ore in a heap leach pad, or below tailings to accelerate consolidation of the tailings can generally be minimized/avoided by using of a suitable protection layer between the GMB and the overlying (Tognon et al. 2000; Brachman and Gudina 2008; Hornsey and Wishaw 2012; Brachman and Sabir 2013; Rowe et al. 2013; Abdelaal et al. 2014; Ewais et al., 2014; Marcotte and Fleming 2020). It follows logically that for a tailing storage facility, a suitable protection layer below the GMB would also provide protection from indentation induced strains caused by gravel in the subgrade.

Nonwoven needle-punched geotextiles (GTXs) are commonly used as a protection/filtration layer between GMB and its underlying/overlying coarse gravels because they are commercially available, easy to install, and economical relative to many of the other options (Rowe 1988, 2005, 2012; Giroud 2016; Lupo 2010; Cazzuffi and Gioffrè 2020). In the tailings storage application where the consolidated tailings have a much lower hydraulic conductivity than natural subgrade materials beneath the GMB, piping is prone to occur when the subgrade soil is filter incompatible with its overlying tailings (Rowe et al. 2017; Chou et al. 2018; Fan and Rowe 2022b). The migration of tailings and the potential piping through any GMB defects can be effectively prevented by introducing a GTX filtration layer that satisfies the retention criterion either above or beneath the GMB (Rowe et al. 2017; Fan and Rowe 2022b). Besides the filtration effect of GTXs, the protection between the GMB and coarse gravels offered by GTXs may comprise two forms. First, as the gravel particle deforms into the GTX, the thickness of the GTX is reduced, and the contact area between gravel particle and GTX increases. This spreads the gravel force over a larger area, resulting in a slightly wider indentation and thereby smaller strains in the GMB relative to no protection. This is commonly referred to as cushioning (Brachman and Sabir 2013). Second, as the GTX deforms, membrane tensions can be mobilized in the GTX, further reducing the contact force applied to the GMB from the gravel particle (Brachman and Sabir 2013). The amount of membrane tension mobilized depends on the slack in, and stiffness of, the GTX together with the magnitude of displacement. Although the filtration effect of GTX was proven to effectively prevent piping through any existing GMB holes in TSFs (Rowe et al. 2017; Fan and Rowe 2022b), and the satisfactory protection effect of GTX in minimizing tensile strains of a GMB in municipal solid waste landfills (Rowe 2005, 2012, 2020; Brachman and Gudina 2008; Brachman and Sabir 2013; Eldesouky and Brachman 2020) and in water impoundments (Giroud 2016; Lupo 2010; Cazzuffi and Gioffrè 2020), the effectiveness and suitability of a GTX as a protection layer in minimizing tensile strains of a GMB for a tailings storage application is unknown.

Thus, the objective of this paper is to quantify the short-term tensile strains induced in a 1.5-mm-thick HDPE GMB from different: (1) subgrades, (2) consolidation stresses, and (3) geotextile protection layers.

2. Experimental Investigation

2.1 Test Apparatus and Method

A cylindrical steel pressure vessel with an inside diameter of 590 mm and a height of 500 mm (Fig. 1) was used to examine the response of a GMB to different subgrade materials. Vertical pressures (σ_v) of 500 kPa, 1000 kPa, and 2000 kPa were applied by hydraulic pressure injected between the steel and the rubber bladder shown in Fig. 1. The steel pressure vessels had a capacity of 3000 kPa. Horizontal pressures corresponding to conditions of zero lateral strain were developed by limiting the outward deflection of the thick walled streel test apparatus. A friction treatment was used to reduce side wall friction along the vertical boundaries of the test apparatus to less that 5% (Tognon et al. 1999; Brachman et al. 2014).

2.2 Geomembrane

A smooth HDPE GMB with a thickness of 1.5 mm was examined. This type and thickness of GMB was one of the most commonly used in recent mining application worldwide (Rowe et al. 2013), presumably because its high strength and excellent chemical resistance to a wide range of chemicals due mainly to its high crystallinity (40% - 60%). The density of the GMB examined was 947 kg/m^3. Additional index tensile properties of the GMB are given in Table 1. All the GMB tested were obtained from the same roll.

2.3 Tailings

The tailings examined, from a mining facility in British Columbia (Canada), was silty sand (denoted as SM in the USCS classification) with 30% nonplastic fines (<75 μm; Table 2 and Fig. 2) and a specific gravity of ~2.65. Based on consolidation tests, the voids ratio – effective stress relationship was given by (Fan and Rowe 2022a; Fan et al. 2022):

$$e = -0.046 ln\sigma'_v + 0.755 \quad (1)$$

2.4 Subgrades

Four subgrades were studied (detail properties are given in Table 2 and Fig. 2):

1. a poorly graded angular to sub-angular gravel (GP) with a uniformity coefficient, $C_u \sim 4$,
2. a well-graded graded angular to sub-angular gravel (GW),

3. a poorly graded subrounded sand (SP) also with $C_u \sim 4$,
4. a silty sand (SM) with 18% nonplastic fines.

The GW subgrade was more well-graded than the GP gravel and the gradation curve converged with GP for particle sizes larger than 6.7 mm. 24% of the GW subgrade was < 6.7 mm and had a minimum grain size (0.6 mm; retained on No. 30 sieve) very close to that for the SP subgrade (0.43 mm; retained on No. 40 sieve). The subgrade materials for GP, GW, and SP were comprised of angular to sub-angular particles arising from crushing stone for particle size larger than 1.18 mm (No. 16 sieve) and sub-angular silica sand for particle size smaller than 1.18 mm (see Fig. 3). As placed, the GP, GW, and SP subgrades were relatively incompressible compared to the compressible, loosely placed, silty sand tailings which experienced about 100 mm of settlement with the increase in stress to 2000 kPa. There was no discernable settlement for GP, GW, and SP subgrades after consolidated at 2000 kPa for around 100 hours. The SM subgrade was cyclone silty sand tailings sourced from the same mining facility as the overlying tailings (Fig. 2 and Table 2).

2.5 Geotextiles

Two nonwoven needle-punched geotextiles, denoted as GTX1 and GTX2 (Table 3) were used as a single protection layer between GMB and the subgrade materials. GTX1 was a needle-punched nonwoven with a random network of 100% virgin polypropylene staple fibers and a mass per unit area, M_a = 450 g/m^2. GTX2 was a needle-punched staple fiber nonwoven product manufactured using blends of polypropylene and polyester resins with M_a = 1420 g/m^2. The apparent opening size (AOS) was 0.15 mm for GTX1 and 0.075 mm for GTX2. Based on the comparison between the particle size of silty sand and the AOS of geotextile, the geotextile satisfied the retention criteria summarized by Gardoni and Palmeira (2002). The two GTXs examined are widely used as the protection layer in the North America. Although much heavier protection GTX is recommended in some regions (e.g., Germany), it is very rarely used in mining application due to cost which exceeds that of the geomembrane, and so this study is directed to illustrating the feasibility of GTX examined herein to reduce tensile strains arising from the subgrades of interest.

2.6 Test Procedure

The 200-mm-thick subgrade was placed in several lifts, with care being taken to avoid segregation during placement. Each lift was tamped using a steel block to produce as flat a surface as possible. The dry density of the GP, GW, and SP subgrades varied between 1700 and 1900 kg/m^3.

Test 8 was conducted to investigate the effect of subgrade stiffness on the GMB indentation and stains (Table 4). In this case, the silty sand subgrade (SM) was compacted in seven 30-mm-thick lifts with a steel block to a density of 2000 kg/m^3 at ~20 % gravimetric water content, which was notably higher than its Standard Proctor optimum moisture content of 11%. This was to simulate the scenario where the cyclone silty sand tailings were used as the subgrade earthwork construction materials for a TSF. For Test 9, the silty sand subgrade (SM) was compacted at the Standard Proctor optimum moisture content of ~11% following the same procedure as that for Test 8.

To study its impact on the GMB local indentation and the resultant tensile strain, some tests were conducted without a GTX protection layer, some with a layer of GTX1 and some with a layer of GTX2 between the subgrade and the GMB (Table 4, Fig. 1). To permanently preserve the deformation of the GMB after removal of the load, two rectangular soft lead sheets, 160 mm wide × 270 mm long each and 0.4-mm-thick, were placed on the upper surface of the GMB. The lead sheet was sufficiently thin and soft so that it did not locally stiffen the response of the GMB as previously demonstrated by several investigators (e.g., Tognon et al. 2000; Brachman and Gudina 2008).

For the tests with GP, GW, and SP subgrades, fully saturated silty sand tailings slurry with approximately 70% solids content was placed above the GMB to a thickness of approximately 300 mm. To prevent any preferential flow around the circumference of the GMB, a bentonite perimeter seal was introduced around the top and bottom of the GMB edges. After 24 hours deposition and settlement of the slurry, a sand leveling layer, wrapped in a separator geotextile, was used to fill the gap between the top of tailings and the rubber bladder. The final thickness of tailings after the consolidation was close to 200 mm. For Tests 8 and 9 in Table 4 with SM subgrade, the overliner tailings was prepared using the same procedure as the SM subgrade at the water content of 12% until reaching a final thickness of 200 mm.

At the start of a test, pressure was applied at a rate of 10 kPa per minute until the target pressure σ_v of 500, 1000, or 2000 kPa was reached (see Table 4). For the tests with GP, GW, and SP subgrades, tailings were consolidated at 250, 500, and 1000 kPa for σ_v of 500, 1000, and 2000 kPa, respectively, by maintaining the pore pressure u of 250, 500, and 1000 kPa, respectively, within the tailings through two drainage ports at the sidewall of the cell (Fig. 1). Adopting a unit weight of water is 9.8 kN/m^3 and the submerged unit weight of tailings of 10 kN/m^3, the simulated tailings thickness, denoted as T, and the water head above the GMB, denoted as H, were 25 m and 25.5 m, respectively, for σ_v = 500 kPa and u = 250 kPa, 50 m and 51 m, respectively, for σ_v = 1000 kPa and u = 500 kPa, and 100 m and 102 m, respectively, for σ_v = 2000 kPa and u = 1000 kPa.

The pressure applied on the GMB, σ_v, was unaffected by the consolidation of tailings since this it was externally applied. However, the stiffness of tailings in contact with the GMB progressively increased with increasing effective stress and this may affect the tensile strains induced in the GMB. The target pressure was held constant for around 100 h. The consolidation of tailings was accelerated by periodically opening the two drainage ports on the sidewall of the cell (Fig. 1). After reaching the target σ_v and u within the cell, 100% consolidation of tailings was reached when pore pressure, u, monitored by pressure transducer did not increase with the closing the sidewall drainage ports, (i.e., no excess pore water migration towards the drainage ports). The 100 h test duration chosen herein was notably greater than the 24 hours required for the consolidation of tailings and hence considered to be adequate to acquire the indentations. These strains represent most of the strains likely to be developed, however, it is acknowledged that there may be further strain increases with additional time due to long-term time-dependant deformation of the subgrade. All the experiments were conducted at a temperature of 21 ± 2 ºC; as such, the strains may underestimate the pressures if service temperatures are higher.

After the completion of a test, the test cell was depressurized and the tailings removed to allow examination of the GMB and the lead sheets. After carefully removing the GMB and lead sheets from the cell, each GMB sample was examined visually for scratches, signs of yielding, and notable indentations. The GMB was visually checked for puncture with back-light in a dark room. A mould of the lead sheet was cast with low-shrinkage plaster of Paris to permanently preserve its deformed shape. The major indentations in the lead sheets were identified and the surface was scanned using a laser scanner to quantify indentations and hence allow the evaluation of the strains using the method of Tognon et al. (2000). Since the post-test indentations were all from the subgrade materials (as discussed later), there was an observation error arising from the thickness of lead sheet above the GMB. The real profile of indentation on the GMB surface was actually widened by the scanned indentation on the upper surface of lead sheet, which slightly underestimated the real tensile strain. As shown by Brachman and Gudina (2008), the small underestimate in tensile strain due to the lead sheet thickness could be neglected for the 0.4-mm-thick lead sheet used.

3. Results: GMB Tensile Strains

The GMB was not punctured in any of these short-term tests; however, significant tensile strains were mobilized in the GMB for some tests. For the tests with GP, GW, and SP subgrades, all the indentations were from the bottom of the GMB and hence were attributed to the subgrade. This is because these subgrades were much stiffer and coarser than the overlying tailings. The GMB tensile strain evaluated using the method of Tognon et al. (2000) considers both the membrane and the bending components of strain. While membrane strain is uniform throughout the thickness of the GMB, bending strain varies from zero at the middle surface of the GMB to being greatest at the extreme fibers (where stress cracking will be initiated). Strains for the subgrades of GP, GW, and SP were calculated for at least 13 of the most prominent indentations in two lead sheets for each test. For Test 8 with SM subgrade compacted at ~20% gravimetric water content, there was only one discernable indentation that could be analyzed; whereas for Test 9 with SM subgrade compacted at the Standard Proctor optimum moisture content of ~11%, no discernable indentation was observed (Fig. 4). The largest three tensile strains from each test are given in Table 4.

3.1 Effect of Subgrade

The seven largest strains calculated from the tests with GP, GW, and SP subgrades are shown in Fig. 5. Subgrade GP was the coarsest examined, leading to the most prominent local tensile strains at the same applied pressure. For example, the maximum tensile strain at 2000 kPa was 32% for GP subgrade, 16% for GW subgrade, 13% for SP subgrade, and ~ 0% for SM subgrade compacted at optimum water content (Table 4).

Subgrade GW contained more finer component (< 6.7 mm) than GP, these finer particles fit in around the larger particles reduced local irregularities in GMB settlement and local indentations in the GMB (see Figs. 6a and 6b). Consequently, the seven largest GMB tensile strains for GW were reduced by an average factor of 1.7 at 2000 kPa, 1.4 at 1000 kPa, and 1.8 at 500 kPa relative to GP, but all cases exceeded a maximum desirable tensile strain from all sources of 5% (Rowe et al. 2019b).

Subgrade SP was the finest examined among GP, GW, and SP subgrades. With the same shaped gradation curve as GP, subgrade SP had smaller maximum and minimum grain sizes (Fig. 2), the resultant seven largest GMB tensile strains for SP were reduced by a factor of 2.6 at 2000 kPa relative to GP (Fig. 5c). Subgrade GW was more well-graded than SP and had a very close minimum grain size (0.6 mm) to that of SP (0.43 mm). However, because of a much larger maximum grain size for GW (63.5 mm) than for SP (9.5 mm) and the consequent greater surface irregularities, the resultant seven largest GMB tensile strains for subgrade GW at 2000 kPa was in average 1.6-fold higher than those for subgrade SP.

Therefore, both the maximum and the minimum subgrade grain sizes affected the local indentations and tensile strains in GMB. Since the subgrade particles were much stiffer than tailings, the particles at the subgrade surface might locally attract force due to the uneven surface arising from the surface irregularity (see Figs. 6a and 6b), resulting in local irregularities in GMB settlement and local indentations in the GMB that may lead to tensile strains. Decreasing the maximum grain size and increasing the finer portion (sand size particles) to fill the gap between the adjacent coarse particles both improved the surface irregularity and reduced the GMB tensile strains.

3.2 Soft Subgrade

The high initial water content (~20%) in Test 8 exploring the scenario of using the cyclone silty sand tailings as the subgrade earthwork construction materials produced a SM subgrade with low stiffness and high compressibility, compared with the lower initial water content (~12%) overlying tailings. During the test, excess pore water within the subgrade was allowed to seep through the outlet drain at the bottom of the steel vessel. Post-test exhumation revealed that there had been some consolidation of the subgrade and the final water content was ~15%. No distinct indentation was observed visually at 500 kPa, showing the negligible impact arising from the differential stiffness between the subgrade and the overliner. Only one indentation with the tensile strain of 2% was detected by the laser scanner. The indentation was likely due to the differential settlement (<1 mm) resulting from minor differences in density of the subgrade. Brachman et al. (2014) experimentally examined the local tensile strains within a 1.5-mm-thick HDPE GMB in heap leach applications. There was a 150-mm-thick silty sand layer, compacted to its Standard Proctor maximum dry density, underlying and overlying the GMB as the subgrade and the protection layer, respectively. The largest tensile strain was no greater than 2% at the vertical pressure of 3000 kPa. Summarizing the findings of Tests 8 and 9 and Brachman et al. (2014), the SM subgrade was very effective at reducing local indentations in the GMB, even when it was compacted at a water content notably higher than its optimum water content.

3.3 Effect of Geotextile Protection Layer

Due to the cushioning effect arising from the GTX, each GMB indentation was widened (see Fig. 6c), reducing the steepness of deformation and tensile strain. The seven largest strains calculated from the tests with GTX protection layer at 2000 kPa are shown in Fig. 7. For the 450 g/m^2 GTX1, the maximum tensile strain at 2000 kPa reduced from 32% to 23% for GP, 16% to 8% for GW, and 13% to 6% for SP; the seven largest GMB tensile strains at 2000 kPa were reduced by a factor of 1.4 for GP subgrade (Fig. 7a), 2.2 for GW subgrade (Fig. 7b), and 2.3 for SP subgrade (Fig. 7c), compared with the corresponding tests without GTX protection. Meanwhile, for the tests with GP subgrade, increasing the pressure from 500 kPa to 1000 kPa, and finally to 2000 kPa, the maximum tensile strain with the 450 g/m^2 GTX1 protection decreased from 14% to 7% at 500 kPa, 17% to 10% at 1000 kPa, and 32% to 23% at 2000 kPa, the seven largest GMB tensile strains were reduced by a factor of 2.2, 1.6, and 1.4, respectively, reflecting the decreasing GTX cushioning effect with the increasing pressure.

Brachman and Gudina (2008) classified contact types between 1.5-mm-thick HDPE GMB and two poorly graded angular gravels into point, edge, area, perimeter, and composite contacts. For two angular gravel subgrades evaluated by Brachman and Gudina (2008), approximately 40% of the contacts were point contacts, the steepest GMB indentations and the largest tensile strains were caused by point and edge contacts. The GTX thickness became smaller with the increasing pressure, point and edge contacts both locally attracted more force than the others contact types, leading to a further reduction in both the GTX thickness and cushioning effect. Therefore, the reduction factor arising from the GTX1 protection layer for the seven largest GMB tensile strains decreased with the increasing pressure.

For Test 3B with the 1420 g/m^2 GTX2 as protection layer, the seven largest GMB tensile strains at 2000 kPa (Fig. 7a) were reduced by a factor of 2.4 compared with those for Test 3 without protection layer, and the maximum strain decreased from 32% to 14%. The strains for Test 3B (GTX2) were notably less than those for Test 3A (GTX1) with the maximum strain of 23% for Test 3A and 14% for Test 3B. This is because with the increasing GTX mass from 450 (GTX1) to 1420 g/m^2 (GTX2), a greater cushioning effect was provided and hence the indentations became wider; also, as the stiffness of the protection layer increased, more membrane tensions were mobilized in the GTX2. Consequently, the protection layer took greater force, less force was transferred to the GMB and the subgrade, resulting in smaller indentations and tensile strains for Test 3B. The seven largest GMB tensile strains at 2000 kPa were very similar between the subgrades of GP + GTX2 and SP (Figs. 7a and 7c), representing the efficacy of geotextile relating to minimizing the tensile strains in a GMB.

Fine tailings consolidate slowly, on the order of decades, resulting in a much greater piping potential through the unconsolidated or partially consolidated tailings in the short term than through the consolidated tailings in the long term. A GTX protection /filtration /separation layer is a practical way of preventing piping at the early stage of a TSF where a filter compatible subgrade is not easy to be achieved. Since this is a temporary need for the GTX, a GTX selected to have adequate filtration characteristics and service life, may be appropriate. However, if the GTX layer is introduced above the GMB, the lateral interface transmissivity of GTX more readily transmits flow to the GMB hole from further away than when the tailings are in direct contact with the GMB, resulting in a 60% increase in the measured leakage through a 10-mm-diameter hole (Rowe et al. 2017). Furthermore, introducing the GTX above the GMB has no significant impact on the GMB indentations and tensile strains since the indentations primarily arise from the bottom of the GMB due to the higher stiffness of the subgrade than the overlying tailings. In contrast, introducing the GTX beneath the GMB slightly decreased leakage through a 50-mm-diameter hole by up to 15% relative to the case without the GTX protection layer (Fan and Rowe 2022b), and notably reduced the GMB tensile strains (Figs. 6c and 7), especially for the GW and SP subgrades, or a thicker GTX. The decrease in leakage may be caused by the clogging of GTX by particles passing through the hole. With a GTX protection layer below the GMB, the leakage through a larger hole was still notably greater than that through a smaller hole, which highlights the importance of avoiding large localized GMB tensile strain to minimize the potential leakage in the long term (the effect of hole size on leakage can be assessed for a circular hole from Fan and Rowe (2022a) and for the more general case of circle, rectangle, or slit from Rowe and Fan (2022)). Thus, if a GTX filter/separator/protector layer is to be used in the tailings storage applications for minimizing the risk of piping and reducing the GMB tensile strain, it should be between the GMB and the subgrade and not between the tailings and GMB.

3.4 Effect of Applied Pressure

The influence of pressure on GMB strain using GP and GW subgrades is shown in Fig. 8. There is an overall trend of the three largest values of strains from each test series increasing with the applied pressure since narrower and deeper indentations arose from larger pressures. There is a poor correlation between the pressure and both the three largest strains and the maximum strain. This is considered to be caused by the variability of the subgrade surface irregularity among different tests for the same type of subgrade, creating different distributions of localized point and edge contacts on the GMB. Due to the GTX cushioning effect and the higher finer component within GW subgrade, the maximum strains for both the GP subgrade with GTX1 and the GW subgrade without GTX were below the maximum strain for GP subgrade at each applied pressure (Fig. 8).

Based on the data available, the relationship between the average three largest tensile strains (%) and applied stress σ_v (kPa; 500 kPa ≤ σ_v ≤ 2000 kPa) can be approximately correlated as follows:

$$strain \text{ for GP} = 0.01\sigma_v + 7 \ (\%) \qquad (2)$$

$$strain \text{ for GW} = 0.005\sigma_v + 6 \ (\%) \qquad (3)$$

The parameters in Eqs. 2 and 3 are highly dependent on the coarser particle within the subgrade, represented by D_{85}, and the shape of the subgrade gradation curve, represented by C_c. As noted that the stress crack is likely to be induced once the minimum strain exceeds 6%. The length of time until stress cracking occurs will be primarily dependent on the magnitude of the strain (generally speaking, the greater the strain the sooner the stress cracking) and the representative stress crack resistance of the material (Rowe et al. 2019a).

3.5 Repeatability of Test Results

The repeatability of test was examined by conducting a duplicate of Test 3 (denoted Test 3R) at 2000 kPa with the coarsest GP subgrade (Table 4) since this was expected to give the largest variability due to fewer, larger, and more variable particles in this subgrade. The tensile strains for the seven most prominent indentations in (Tests 3 and 3R) were (32%, 30%), (29%, 27%), (25%, 26%), (22%, 26%), (22%, 26%), (21%, 24%,) and (20%, 24%). Although the maximum tensile strain of 30% for Test 3R was slightly less than 32% for Test 3, the average of both three and seven maximum tensile strains for both tests were close. The difference in the average of the 7 largest strains (24% and 26%) was 2% (i.e., 11% of the strain measured). Therefore, the aforementioned conclusions also apply to Test 3R. The number of the indentations/m2 with the tensile strain ≥ 6% was 670 for Test 3R and was 463 for Test 3, and the number of the indentations per square meter GMB with the tensile strain ≥ 12% was 648 for Test 3R and was 394 for Test 3. Thus, more stress cracking is to be expected for the subgrade produced in Test 3R. The particle sizes for the GP examined varied from the smallest value of 3.35 mm to the largest value of 63.5 mm (Figure 2). The orientations of those angular to sub-angular particles may lead to different contact types (e.g., point, edge, area, and perimeter) with the overlying GMB, leading to a notable difference in GMB tensile strains and variation in strain distribution.

4. Practical Implications

There were no punctures due to the subgrade in any of the cases tested and hence negligible leakage in the short-term due to the subgrade, although there may be short term leakage due to other defects (e.g., defective seams). However, eventually stress cracking can be expected at all locations with tensile strains in excess of about 6% (for both HDPE and LLDPE), with it occurring sooner by the larger strain. To quantify the distribution of strains arising from the subgrade conditions, the number of the indentations/m^2 with the tensile strain ≥ 5% was predicted based on the scanned indentations in the two rectangular lead sheets with the dimension of 160 mm × 270 mm each as summarized in Fig. 9. Table 5 gives the number of tensile strains ≥ 6% for applied pressures of 500, 1000, and 2000 kPa. At 2000 kPa, there were ~ 394 tensile strains exceeding 12% per m^2 and 463 tensile strains/m^2 exceeding 6% for GP. There were ~128 and ~324 tensile strains/m^2 exceeding 12% and 6%, respectively, for GP + GTX1, while increasing the geotextile thickness reduce that to ~ 23 exceeding 12% and 127 exceeding 6% tensile strains/m^2 for GP+GTX2. For the GW subgrade, there were ~ 197 exceeding 12% and 394 exceeding 6% tensile strains/m^2, while adding the geotextile (GW + GTX1) reduce this to ~ 139 tensile strains/m^2 exceeding 6%. For SP there were ~ 15 and 174 tensile strains/m^2 exceeding 12% and 6%, respectively, and adding GTX1 reduce this to ~ 23 tensile strains/m^2 exceeding 6% for SP + GTX1, illustrating the effect of the subgrade sand size particle and GTX on reducing the GMB tensile strain.

GP + GTX1 outperformed GW regarding the number of indentations with tensile strains > 6%, however, both the number of strains >15% and the maximum strain for GP + GTX1 were greater than those for GW; whereas GP + GTX2 had a similar strain distribution as SP alone and GW + GTX1 outperformed SP (Fig. 9). Therefore, better protection effect was achieved by using a thicker GTX; however, placing the GTX protection layer beneath the GMB does not guarantee a better performance than increasing the proportion of sand size particle in the subgrade. The effectiveness and capability of GTX should be assessed by conducting a test similar to those described herein for the anticipated subgrade, GTX, GMB and tailings to assess the benefit of the proposed geotextile in a given situation.

Every indentation yielding a tensile strain greater than 6% there will eventually be over 10,000 stress cracks per hectare, although the time to stress cracking (service life) will increase with the fewest strains in excess of 6% and the higher the representative stress crack resistance SCR_m of the GMB (Rowe et al. 2019b).

The only design scenario examined that is likely to offer a very long service life is to use the SM as the subgrade. The number holes must be considered in the context of the leakage that would occur. Based on stress cracks observed by Ewais et al. (2014), Abdelaal et al. (2014), and Rowe and Fan (2022), three stress crack sizes (i.e., 10 mm

× 0.5 mm, 20 mm × 1.6 mm, and 30 mm × 3.75 mm) were considered, with the number of stress cracks predicted per ha for the different subgrades and applied pressures in Table 5. The leakage was calculated using tailings parameters and the model proposed by Rowe and Fan (2022), and neglected the effect arising from the adjacent defects.

With SM subgrade, no subgrade induced stress cracking is anticipated and with an appropriate geomembrane a long service life with minimal leakage can be anticipated at all three stress levels examined. Wherever possible, a similar or better subgrade is recommended. However, that will not always be possible.

For the GW subgrade at σ_v = 500 kPa, the calculated leakage ranges between 79,000 and 785,000 liters per hectare per day (lphd). To put this into context, based on Beck (2015) less than 5% of composite liners in New York State landfills had leakage exceeding 1,000 lphd, illustrating the inadequacy of GW subgrade as bedding soil for the GMB liner. When the stress is increased to 2000 kPa for the same GW subgrade the leakage increases to between about 790,000 and 7,804,000 lphd. If the nature of the subgrade cannot be readily changed, then the addition of the geotextile protection layer offers some benefit in reducing strains although the long-term survivability of the geotextile needs to be seriously considered and the leakage is still very large.

For the GP subgrade at σ_v = 500 kPa, the calculated leakage ranges between 265,000 and 2,618,000 liters per hectare per day (lphd). When the stress is increased to 2000 kPa for the same GP subgrade, the leakage increases to between about 929,000 and 9,182,000 lphd. Again, the addition of the geotextile protection layer offers some benefit in reducing strains although, again, the long-term survivability of the geotextile needs to be seriously considered, the leakages are still large.

For the SP subgrade at σ_v = 2000 kPa the leakage increases to between about 348,000 and 3,443,000 lphd. This highlights the critical long-term impact of gravel in the subgrade, without sufficient finer material, can have on long-term liner leakage. For all of the subgrades except SM, both with and without the geotextile, contaminant impact calculations would be required to assess the consequences of the magnitude of the calculated leakage.

While there maybe time dependent increases in strain above those obtained in a 100-hour test, any strain exceeding 6% can be considered problematic to the long-term performance of the geomembrane and needs to be avoided if long-term performance is required. The two SM subgrades compacted at water contents of 11% (i.e., optimum water content and compaction) and 20% (i.e., soft subgrade) were both satisfactory for minimizing the tensile strains induced in the GMB. At some facilities some sandy tailings can be used as subgrade for a geomembrane to contain more aggressive (e.g., pyritic) tailings. Where a suitable subgrade is not available or can not be obtained for local quarries, use of sand tailing, or manufacture by sieving unsuitable local soils, the unevenness of the surface can be improved by heavy compaction to minimize subgrade surface irregularity arising from the surface unevenness due to protruding particles. If heavy rolling is not sufficient, consideration may be given to placing a layer GTX above the subgrade below the geomembrane to reduce strains. However there is a serious question as to long-term performance of these geotextiles and hence they are not recommended for this purpose, although they may be useful to minimize the risk of piping of tailings in the shorter term. Since this is a temporary need for the GTX, a suitable GTX, selected to have adequate filtration characteristics and service life, may be appropriate. Two other potential solutions that may be combined with heavy rolling the subgrade include (a) distributing a layer of soil with a maximum particle size of ~ 2mm over the surface to sufficient thickness to prevent excessive strains, or (b) placing a GCL with 4800 g/m² of dry bentonite between the subgrade and the geomembrane. In both cases, tests should be conducted to confirm suitability of the proposed solution at the expected applied stress.

5. Summary and Conclusions

Experiments were conducted to quantify the short-term tensile strains induced in a 1.5-mm-thick HDPE geomembrane (GMB). Four subgrades, a poorly graded gravel (GP), a well-graded gravel (GW), a poorly graded sand (SP), and silty sand (SM), and two different nonwoven needle-punched geotextiles with mass per unit area of 450 g/m² (GTX1) and 1420 g/m² (GTX2) were evaluated. The tensile strains were measured at the applied vertical pressures of 500, 1000, and 2000 kPa for 100 h at a temperature of 21 ± 2 ºC. For the specific conditions and materials examined, the following conclusions were reached:

1) No puncture was observed.
2) The GP subgrade was the coarsest material and had ~ 460 tensile strains/m²

exceeding 6% and ~400 tensile strains/m^2 exceeding 12% at 2000 kPa. This has the capacity to generate 4.6 million holes per hectare with time and leakages up to 9 million lphd that would require a contaminant impact assessment.

3) The GW subgrade had the same 76% coarse fraction (≥ 6.7 mm) as GP, but was more well-graded and contained more sand size particles with a similar minimum grain size as that for SP. At 2000 kPa, it generated ~ 390 tensile strains/m^2 exceeding 6% that can be expected to generate 3.9 million holes per hectare with time and leakages likely to be up to 7.8 million lphd.

4) The finer SP subgrade had same shaped gradation curve as GP, and this reduced the number of tensile strains/m^2 exceeding 6% to about 174, but this could still generate 174,000 holes per hectare with time and leakages up to about 3.4 million lphd.

5) For the SM subgrade, the tensile strain no larger than 2% was observed at 2000 kPa. Thus, the silty sand subgrade was very effective in reducing local indentations in the GMB and providing a very long service life for an appropriately selected HDPE geomembrane.

6) While both the 450 g/m^2 GTX1 and 1420 g/m^2 GTX2 protection reduced the maximum tensile strain. However, the leakages were still relatively large (varying from 46,000 lphd to 6,400,000 lphd) assuming strains exceeding 6% would result in a stress crack without even considering the long-term survivability of the geotextile. For both reasons, the use of the geotextile tested herein to mitigate the unsatisfactory subgrade is unlikely to be a good long-term option for conditions

similar to those examined.

7) An appropriate HDPE or LLDPE geomembrane can be expected to perform very well limiting leakage levels for an extremely long time (Rowe 2020), provided they are well constructed on a suitable subgrade that does not generate significant (>5%) tensile strain in the geomembrane.

Acknowledgements

The research reported in this paper was supported by the Natural Sciences and Engineering Research Council of Canada (NSERC) under Strategic Grant STPGP 521237–18. The tailings tested were obtained and shipped to Queen's for testing by Klohn Crippen Berger. The value of help from Yu Yan Li at Queen's is gratefully acknowledged.

Competing Interests

The authors declare there are no competing interests.

Data Availability Statement

Data generated or analyzed during this study are provided in full within the published article.

References

Abdelaal, F. B., Rowe, R. K., and Brachman, R. W. I. (2014). Brittle rupture of an aged HPDE geomembrane at local gravel indentations under simulated field conditions. *Geosynthetics International*, 21(1), 1-23.

ASTM. (2006). Standard test method for melting and crystallization temperatures by thermal analysis. *ASTM E794*, West Conshohocken, USA.

ASTM. (2010). Standard test method for determining tensile properties of nonreinforced polyethylene and nonreinforced flexible polypropylene geomembranes. *ASTM D6693*, West Conshohocken, USA.

ASTM. (2015). Standard Test Method for Trapezoid Tearing Strength of Geotextiles. *ASTM D4533*. West Conshohocken, USA.

ASTM. (2019). Standard Test Method for Breaking Force and Elongation of Textile Fabrics (Strip Method). *ASTM D5035*. West Conshohocken, USA.

ASTM. (2019). Standard Test Method for Measuring the Nominal Thickness of Geosynthetics. *ASTM D5199*. West Conshohocken, USA.

ASTM. (2020). Standard Test Methods for Mass Per Unit Area (Weight) of Fabric. *ASTM D3776*. West Conshohocken, USA.

ASTM. (2020). Standard Test Method for Determining Apparent Opening Size of a Geotextile. *ASTM D4751*. West Conshohocken, USA.

ASTM. (2020). Standard Test Method for Index Puncture Resistance of Geomembranes and Related Products. *ASTM D4833*. West Conshohocken, USA.

Adesokan, D., Fleming, I., and Hammerlindl, A. (2021). One-dimensional (1D) immediate compression and creep in large particle-sized tire-derived aggregate (TDA) for leachate collection and removal systems (LCRSs). *Canadian Geotechnical Journal*, 58(7), 982-994.

Beck, A. (2015). Available technologies to approach zero leaks. In *Proceedings of the*

Geosynthetics 2015 Conference, Industrial Fabrics Association International, Roseville.

Brachman, R. W. I., and Gudina, S. (2008). Gravel contacts and geomembrane strains for a GM/CCL composite liner. *Geotextiles and Geomembranes*, 26(6), 448-459.

Brachman, R. W. I., and Sabir, A. (2010). Geomembrane puncture and strains from stones in an underlying clay layer. *Geotextiles and Geomembranes,* 28 (4), 335–343.

Brachman, R. W. I., and Sabir, A. (2013). Long-term assessment of a layered-geotextile protection layer for geomembranes. *Journal of geotechnical and geoenvironmental engineering*, 139(5), 752-764.

Brachman, R. W. I., Rowe, R. K., and Irfan, H. (2014). Short-term local tensile strains in HDPE heap leach geomembranes from coarse overliner materials. *Journal of Geotechnical and Geoenvironmental Engineering*, 140(5), 04014011.

Cazzuffi, D., & Gioffrè, D. (2020). Lifetime assessment of exposed PVC-P geomembranes installed on Italian dams. Geotextiles and Geomembranes, 48(2), 130-136.

Chou, Y. C., Rowe, R. K., and Brachman, R. W. (2018). Erosion of silty sand tailings through a geomembrane defect under filter incompatible conditions. *Canadian Geotechnical Journal*, 55(11), 1564-1576.

Davies, M. P., Lighthall, P. C., Rice, S., and Martin, T. E. (2002). Design of tailings dams and impoundments. Keynote address, Tailings and Mine Waste Practices SME, AGM Phoenix, 1-18.

Eldesouky, H. M. G., and Brachman, R. W. I. (2020). Viscoplastic modelling of HDPE geomembrane local stresses and strains. *Geotextiles and Geomembranes*, 48(1), 41-51.

Ewais, A. M. R., Rowe, R. K., Brachman, R. W. I., and Arnepalli, D. N. (2014). Service life of a high-density polyethylene geomembrane under simulated landfill conditions at 85° C. *Journal of Geotechnical and Geoenvironmental Engineering*, 140(11), 04014060.

Fan, J. Y., and Rowe, R. K. (2022a). Seepage through a circular geomembrane hole when covered by fine-grained tailings under filter incompatible conditions. *Canadian Geotechnical Journal*, 59(3), 410-423.

Fan, J. Y., and Rowe, R. K. (2022b). Piping of silty sand tailings through a circular geomembrane hole. *Geotextiles and Geomembranes*, 50(1), 183-196.

Fan, J. Y., Rowe, R. K., and Brachman, R. W. I. (2022). Compressibility and permeability of sand-silt tailings mixtures. *Canadian Geotechnical Journal* (in press).

Gardoni, M. G., and Palmeira, E. M. (2002). Microstructure and pore characteristics of synthetic filters under confinement. *Geotechnique*, 52(6), 405-418.

Giroud, J. P. (1997). Equations for calculating the rate of liquid migration through composite liners due to geomembrane defects. *Geosynthetics International*, 4(3-4), 335-348.

Giroud, J. P. (2016). Leakage control using geomembrane liners. *Soils and Rocks*, 39(3), 213-235.

Giroud, J. P., and Bonaparte, R. (1989a). Leakage through liners constructed with geomembranes—part I. Geomembrane liners. *Geotextiles and Geomembranes*, 8(1), 27-67.

Giroud, J. P., and Bonaparte, R. (1989b). Leakage through liners constructed with geomembranes—Part II. Composite liners. *Geotextiles and Geomembranes*, 8(2), 71-111.

Hornsey, W. P., and Wishaw, D. M. (2012). Development of a methodology for the evaluation of geomembrane strain and relative performance of cushion geotextiles. *Geotextiles and Geomembranes*, 35, 87-99.

Lupo, J. F., and Morrison, K. F. (2007). Geosynthetic design and construction approaches in the mining industry. *Geotextiles and Geomembranes*, 25(2), 96-108.

Lupo, J. F. (2010). Liner system design for heap leach pads. *Geotextiles and Geomembranes*, 28(2), 163-173.

Marcotte, B. A., and Fleming, I. R. (2019). The role of undrained clay soil subgrade properties in controlling deformations in geomembranes. *Geotextiles and Geomembranes*, 47(3), 327-335.

Marcotte, B. A., and Fleming, I. R. (2020). Damage to geomembrane liners from tire derived aggregate. *Geotextiles and Geomembranes*, 48(2), 198-209.

McLeod, H. (2016). History of Tailings Dam Design, Innovation, and Practice Changes Required in the Wake of the Mount Polley Mine Tailings Breach. *GeoVancouver*. Vancouver, Canada.

Peggs, I.D., Schmucker, B., and Carey, P. (2005). Assessment of maximum allowable strains in polyethylene and polypropylene geomembranes. *In Proceedings of the Geo-Frontiers 2005*. American Society of Civil Engineers, Reston, VA.

Peggs, I. D., Gassner, F., Scheirs, J., Tan, D., Arango, A. M. N. and Burkard, B. (2014). Is there a resurgence of stress cracking in HDPE geomembranes. *Proceedings 10th International Geosynthetics Conference*, Berlin, Germany, DGGT, Essen, Germany (CD-ROM).

Rowe, R. K. (1998). Geosynthetics and the minimization of contaminant migration through barrier systems beneath solid waste. *In Proceedings 6th International Conference on Geosynthetics*, Atlanta 1, 27–103.

Rowe, R. K. (2005). Long-term performance of contaminant barrier systems. *Geotechnique*, 55(9), 631-678.

Rowe, R. K. (2012). Short and long-term leakage through composite liners. *Canadian Geotechnical Journal*, 49(2), 141-169.

Rowe, R. K. (2020). Protecting the Environment with Geosynthetics: 53rd Karl Terzaghi Lecture. *Journal of Geotechnical and Geoenvironmental Engineering*, 146(9), 04020081.

Rowe, R. K., and Fan, J. Y. (2021). Effect of geomembrane hole geometry on leakage overlain by saturated tailings. *Geotextiles and Geomembranes*, 49(6), 1506-1518.

Rowe, R. K., and Fan, J. Y. (2022). A general solution for leakage through geomembrane defects overlain by saturated tailings and underlain by highly permeable subgrade. *Geotextiles and Geomembranes*, 50(4), 694-707.

Rowe, R. K., and Yu, Y. (2019). Magnitude and significance of tensile strains in geomembrane landfill liners. *Geotextiles and Geomembranes*, 47(3), 439-458.

Rowe, R. K., Brachman, R. W. I., Irfan, H., Smith, M. E., and Thiel, R. (2013). Effect of underliner on geomembrane strains in heap leach applications. *Geotextiles and Geomembranes*, 40, 37-47.

Rowe, R. K., Joshi, P., Brachman, R. W. I., and McLeod, H. (2017). Leakage through holes in geomembranes below saturated tailings. *Journal of Geotechnical and Geoenvironmental Engineering*, 143(2), 04016099.

Rowe, R.K., Morsy, M.S. and Ewais, A.M.R. (2019a) A Representative Stress Crack Resistance for Polyolefin Geomembranes Used in Waste Management, *Waste Management*, **100**:18-27, https://doi.org/10.1016/j.wasman.2019.08.028

Rowe, R.K., Priyanto, D., Poonan, R. (2019b). Factors affecting the design life of HDPE geomembranes in an LLW disposal facility. In: WM2019 Conference, Phoenix, Arizona, USA, 15p.

Seeger, S., Müller, W. (2003). Theoretical approach to designing protection: selecting a geomembrane strain criterion. In: Dixon, N., Smith, D.M., Greenwood, J.H., Jones, D.R.V. (Eds.), Geosynthetics: Protecting the Environment. Thomas Telford, London, pp. 137–152.

Thiel, R., and Smith, M. E. (2004). State of the practice review of heap leach pad design issues. *Geotextiles and Geomembranes*, 22(6), 555-568.

Tognon, A. R., Rowe, R. K., and Brachman, R. W. (1999). Evaluation of side wall friction for a buried pipe testing facility. *Geotextiles and Geomembranes*, 17(4), 193-212.

Tognon, A. R., Rowe, R. K., and Moore, I. D. (2000). Geomembrane strain observed in large-scale testing of protection layers. *Journal of Geotechnical and Geoenvironmental Engineering*, 126 (12), 1194–1208.

Touze, N. (2020). Healing the world: a geosynthetics solution. *Geosynthetics International*, 1-31.

Touze-Foltz, N., Lupo, J., and Barroso, M. (2008). Geoenvironmental applications of geosynthetics. Keynote Lecture, *Proceedings Eurogeo*, 4, 98.

Table 1. Geomembrane index tensile properties (measured following ASTM D6693 unless otherwise noted)

Property	Direction	Mean	Standard deviation
Yield strength (kN/m)	Machine	29	1
Break strength (kN/m)		47	2
Yield strain (%)		22	1
Break strain (%)		820	30
Yield strength (kN/m)	Cross-machine	31	0.5
Break strength (kN/m)		47	2
Yield strain (%)		18	0.5
Break strain (%)		870	50
Crystallinity (%) (ASTM E794)		52	0.5

Table 2. Properties of tailings and subgrade tested

Material	D_{10} (mm)	D_{30} (mm)	D_{60} (mm)	D_{85} (mm)	C_u	C_c
Tailings	0.02	0.07	0.19	0.4	9.8	1.4
GP subgrade	4.7	8.3	18.8	37.7	4.0	0.8
GW subgrade	2.1	8.3	18.8	37.7	8.8	1.7
SP subgrade	0.75	1.3	3.0	6.0	4.0	0.8
SM subgrade	0.03	0.12	0.23	0.4	6.5	1.7

Note: D_{10}, D_{30}, D_{60}, and D_{85} represent the diameter of grain size at which 10%, 30%, 60%, and 85% by mass is finer, respectively. C_u is the coefficient of uniformity. C_c is the coefficient of curvature.

Table 3. Index properties of examined nonwoven needle-punched geotextiles

Property	Method	Unit	GTX designation (mean ± standard deviation) GTX1	GTX2
Mass per unit area	ASTM D3776	g/m^2	450	1420
Thickness	ASTM D5199	mm	3.5	6.4
Tensile peak strength	ASTM D5035	N	805 ± 40	1820 ± 130
Elongation at peak tensile strength	ASTM D5035	mm	60 ± 10	85 ± 20
Tensile break strength	ASTM D5035	N	780 ± 40	1440 ± 90
Elongation at break tensile strength	ASTM D5035	mm	60 ± 10	85 ± 20
Puncture resistance	ASTM D4833	N	1660 ± 320	2720 ± 130
Tear strength	ASTM D4533	N	2340 ± 110	3200 ± 40
AOS	ASTM D4751	µm	150	75

Table 4. Test conditions for GMB tensile strain and three largest strains for each test

Test No.	Underliner	Applied pressure σ_v (kPa)	No. of indentation scanned	No. of strain* ≥ 6%	Largest tensile strain (%)		
					a	*b*	*c*
1	GP	500	30	30[b]	14	14	12
1A	GP+GTX1	500	23	6	7	6	6
2	GP	1000	25	24	17	16	14
2A	GP+GTX1	1000	28	20	10	9	9
3	GP	2000	40	40[b]	32	29	25
3R[e]	GP	2000	58	58[e]	30	27	26
3A	GP+GTX1	2000	29	28	23	22	19
3B	GP+GTX2	2000	24	11	14	12	11
4	GW	500	23	9	9	8	8
5	GW	1000	20	14	14	12	10
6	GW	2000	36	34	16	15	15
6A	GW+GTX1	2000	19	12	8	8	7
7	SP	2000	24	15	13	11	9
7A	SP+GTX1	2000	13	2	6	6	5
8	SM[c]	500	1	0	2	N/A[a]	N/A[a]
9	SM[d]	2000	1	0	N/A[a]	N/A[a]	N/A[a]

Note: * In an area of 0.0864 m^2. [a]No discernable indentation. [b]The minimum scanned strain was 6%. [c]The underliner was compacted at ~20 % gravimetric water content (the Standard Proctor optimum moisture content was 11%). [d]The underliner was compacted at the Standard Proctor optimum moisture content of ~11%. [e]Repeat test, the minimum scanned strain for those 58 indentations analyzed was 7%.

Table 5. Expected leakage for stress cracks of three assumed sizes

σ_v (kPa)	Subgrade	Strains ≥ 6% (#/m²)	(#/ha)	L = 10 mm B = 0.5 mm Q (lphd)	L = 20 mm B = 1.6 mm Q (lphd)	L = 30 mm B = 1.75 mm Q (lphd)
500	GP	347	3,470,000	265,000	1,133,000	2,618,000
500	GP+GTX1	69	694,000	53,000	227,000	524,000
500	GW	104	1,040,000	79,000	340,000	785,000
500	SM	0	0	-	-	-
1000	GP	289	2,890,000	367,000	1,568,000	3,625,000
1000	GP+GTX1	231	2,310,000	293,000	1,255,000	2,900,000
1000	GW	162	1,620,000	205,000	878,000	2,030,000
2000	GP	463	4,630,000	929,000	3,973,000	9,182,000
2000	GP+GTX1	324	3,240,000	650,000	2,781,000	6,427,000
2000	GP+GTX2	127	1,270,000	255,000	1,093,000	2,525,000
2000	GW	394	3,940,000	790,000	3,377,000	7,804,000
2000	GW+GTX1	139	1,390,000	279,000	1,192,000	2,754,000
2000	SP	174	1,770,000	348,000	1,490,000	3,443,000
2000	SP+GTX1	23	230,000	46,000	199,000	459,000
2000	SM	0	0	-	-	-

t= 1.5 mm, k_2/k_1 =1.17, k_1 = 1.5x10^{-8} m/s at σ_v =500kPa, T= 25 m, H=26 m; k_1 = 1.2x10^{-8} m/s at σ_v =1,000kPa, T= 50 m, H=54 m; k_1 = 0.95x10^{-8} m/s at σ_v =2,000kPa, T= 100 m, H= 108 m (Note: t is GMB thickness, k_1 is hydraulic conductivity within the GMB defect and predicted based on the empirical relationship by Rowe and Fan (2022), k_2 is the hydraulic conductivity for tailings directly above the defect, T is the tailings thickiness, H is the water head above the GMB, L is the equivalent rectangular length of the stress crack, B is the equivalent rectangular width of the stress crack, Q is the predicted leakage based on the method summarized by Rowe and Fan (2022))

Figure Captions

Fig. 1. Cross section through a typical test cell used in experiments (modified from Fan and Rowe 2022b)

Fig. 2. Grain size distributions of silty sand tailings and four subgrade materials

Fig. 3. Particle shapes from subgrades: (a) GP; (b) GW; (c) SP

Fig. 4. Photographs showing a 160 mm × 270 mm region of the lead sheet in Test 9 with SM subgrade compacted at the Standard Proctor optimum moisture content for: (a) before the experiment, and (b) after applying the 2000 kPa consolidation stress for over 100 hours

Fig. 5. Seven largest strains calculated from each test showing the effect of subgrade for: (a) Tests 1 and 4 at 500 kPa, (b) Tests 2 and 5 at 1000 kPa, and (c) Tests 3, 6 and 7 at 2000 kPa

Fig. 6. a) Illustration of coarse gravel (GP) contact leading to higher local indentations in a GMB. b) Illustration of the impact of finer component in reducing local indentations in a GMB. c) Illustration of the impact of GTX protection layer between coarse gravel and GMB in reducing local indentations.

Fig. 7. Effectiveness of geotextile (GTX) protection layer between the GMB and subgrade on reducing tensile strain at 2000 kPa for: (a) Tests 3, 3A and 3B, (b) Tests 6 and 6A, and (c) Tests 7 and 7A

Fig. 8. Three largest strains calculated from each test showing the effect of pressure, subgrade, and GTX protection layer

Fig. 9. Distributions of GMB tensile strains ≥ 5% per square meter GMB with subgrades of GP, GW, and SP at 2000 kPa

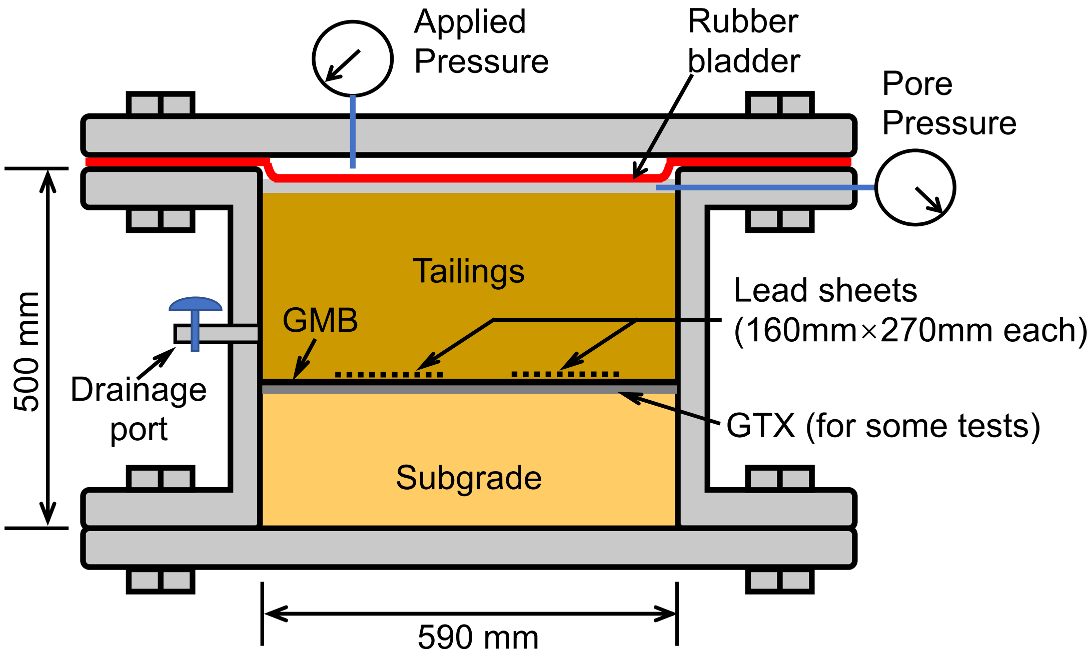

Fig. 1. Cross section through a typical test cell used in experiments (modified from Fan and Rowe 2022b)

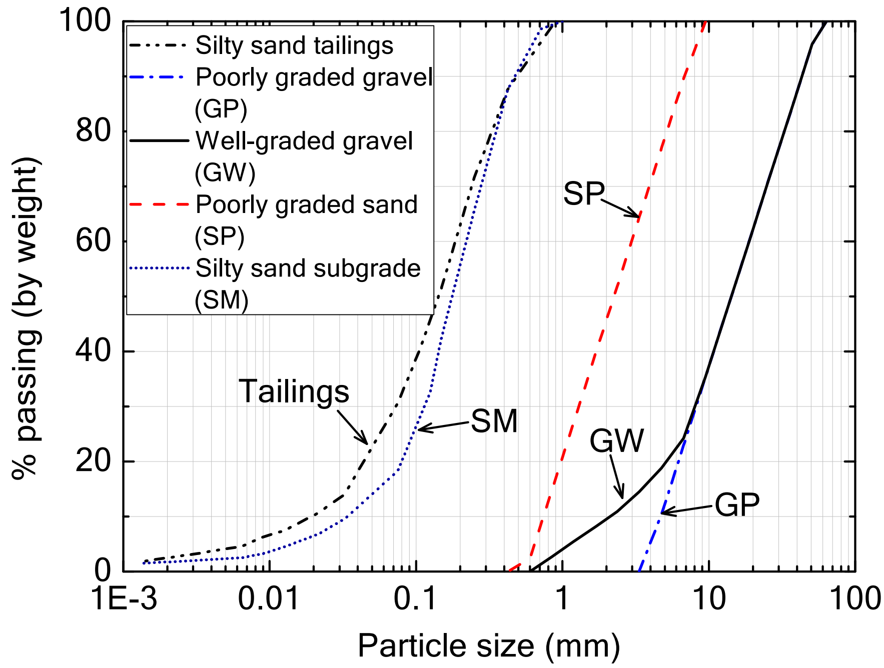

Fig. 2. Grain size distributions of silty sand tailings and four subgrade materials

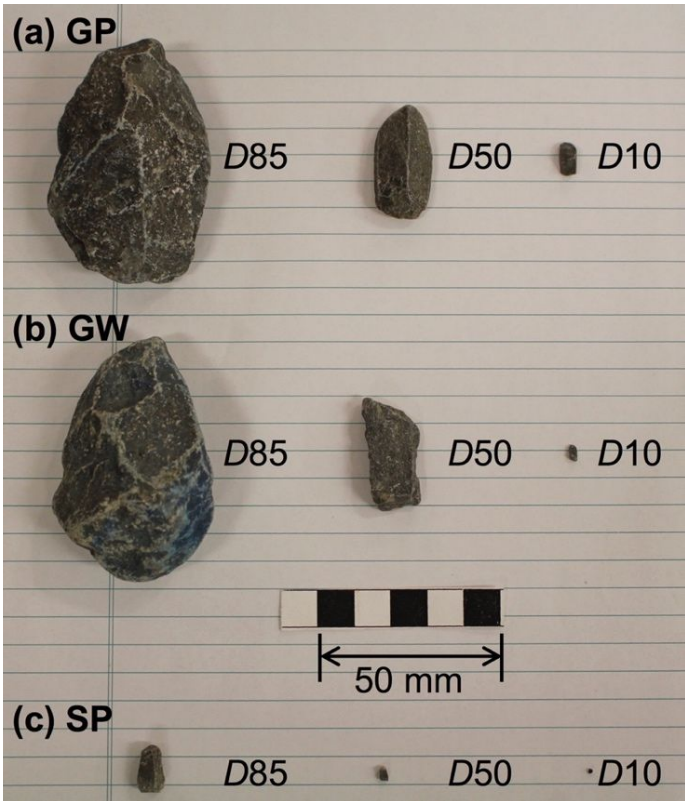

Fig. 3. Particle shapes from subgrades: (a) GP; (b) GW; (c) SP

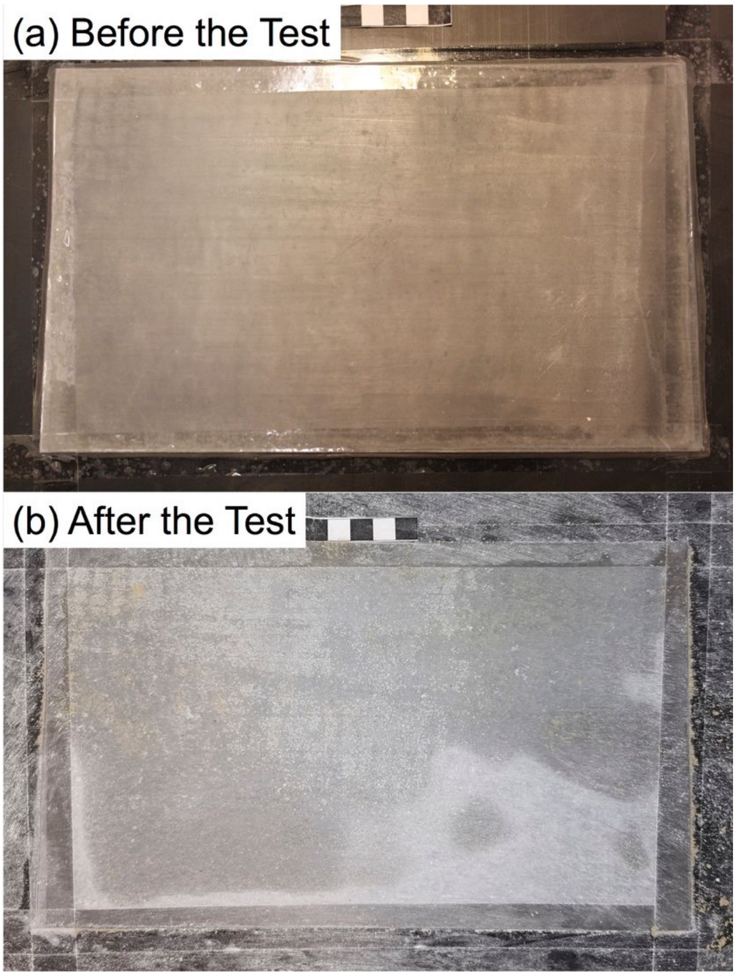

Fig. 4. Photographs showing a 160 mm × 270 mm region of the lead sheet in Test 9 with SM subgrade compacted at the Standard Proctor optimum moisture content for: (a) before the experiment, and (b) after applying the 2000 kPa consolidation stress for over 100 hours

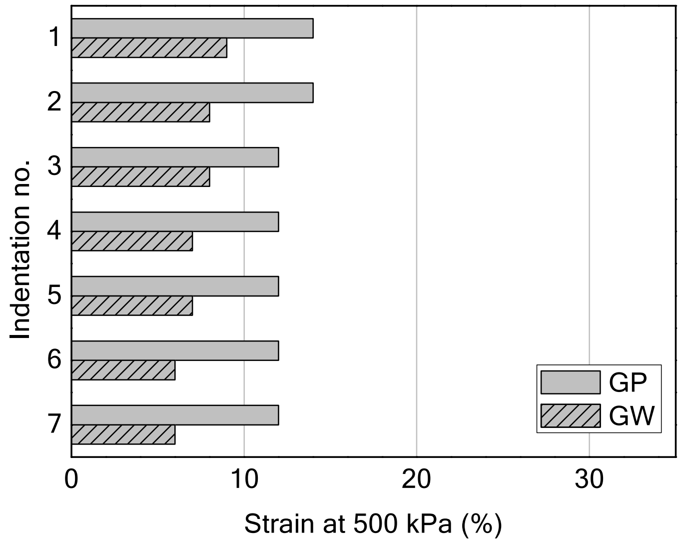

(a) Tests 1 and 4

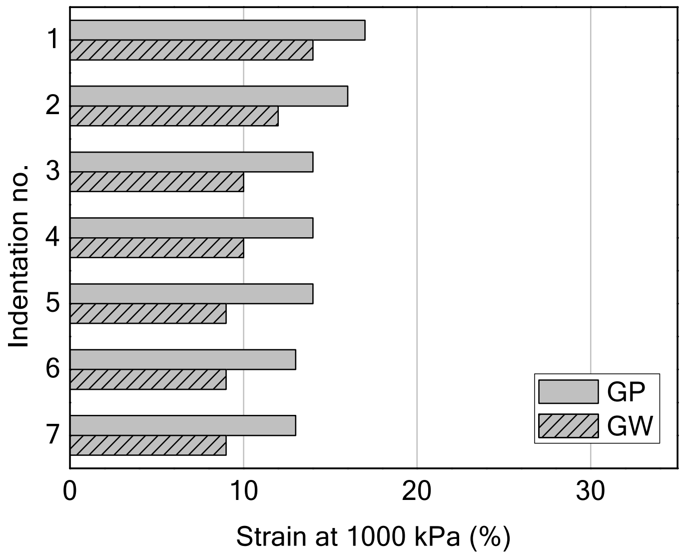

(b) Tests 2 and 5

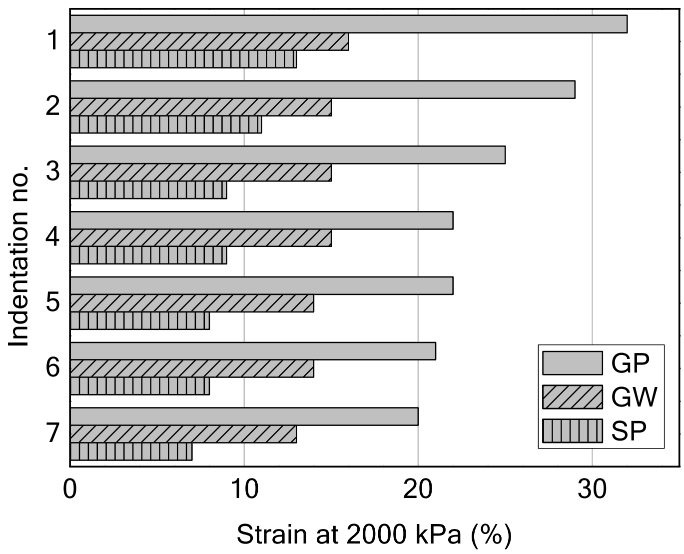

(c) Tests 3, 6 and 7

Fig. 5. Seven largest strains calculated from each test showing the effect of subgrade for: (a) Tests 1 and 4 at 500 kPa, (b) Tests 2 and 5 at 1000 kPa, and (c) Tests 3, 6 and 7 at 2000 kPa

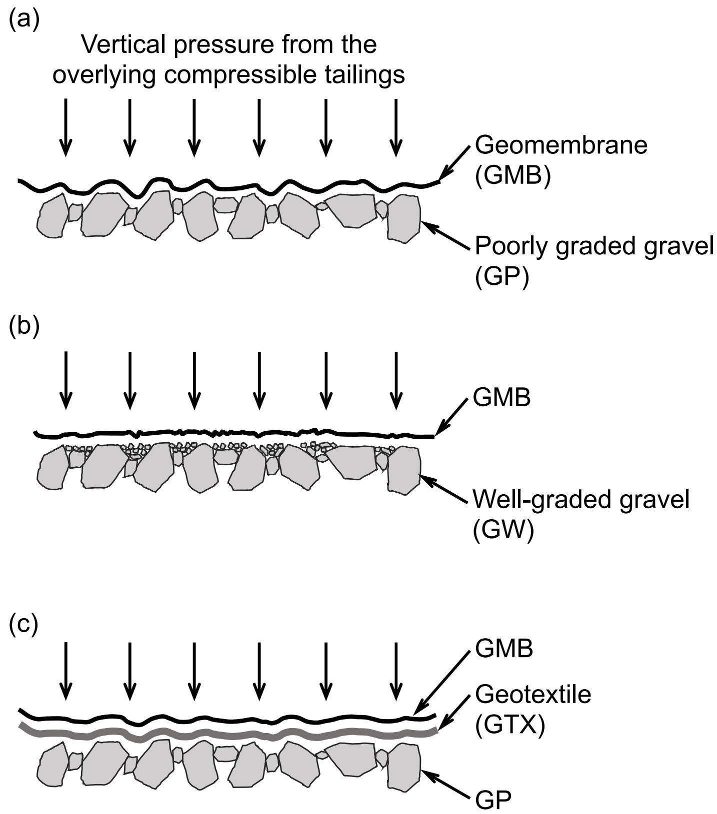

Fig. 6. a) Illustration of coarse gravel (GP) contact leading to higher local indentations in a GMB. b) Illustration of the impact of finer component in reducing local indentations in a GMB. c) Illustration of the impact of GTX protection layer between coarse gravel and GMB in reducing local indentations.

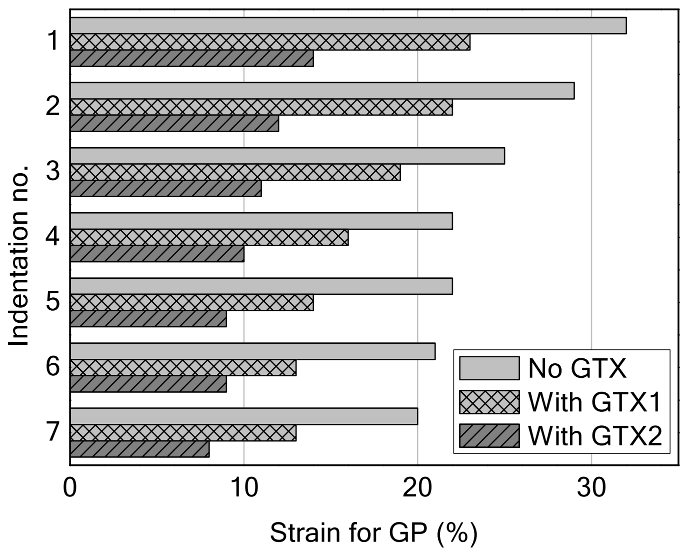

(a) Tests 3, 3A and 3B

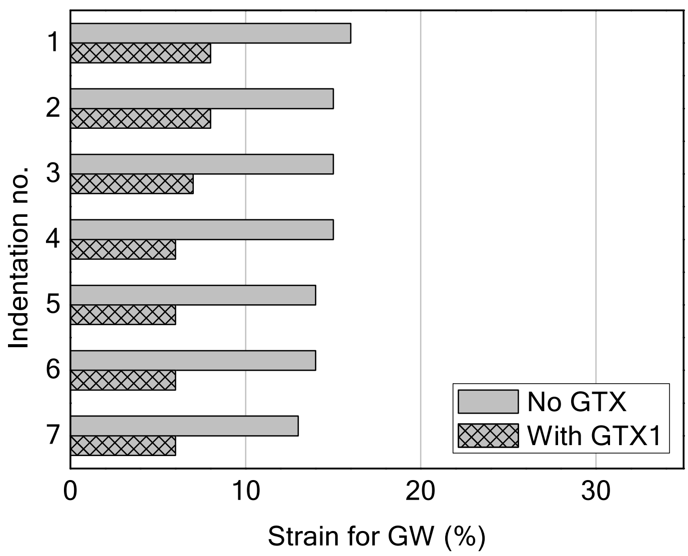

(b) Tests 6 and 6A

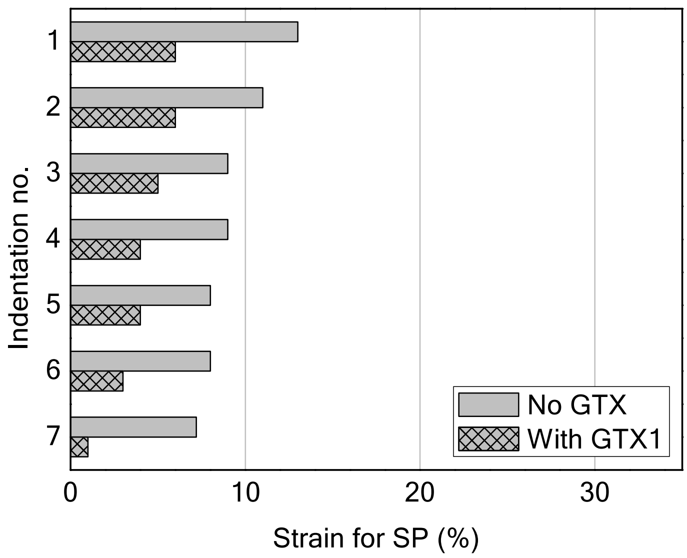

(c) Tests 7 and 7A

Fig. 7. Effectiveness of geotextile (GTX) protection layer between the GMB and subgrade on reducing tensile strain at 2000 kPa for: (a) Tests 3, 3A and 3B, (b) Tests 6 and 6A, and (c) Tests 7 and 7A

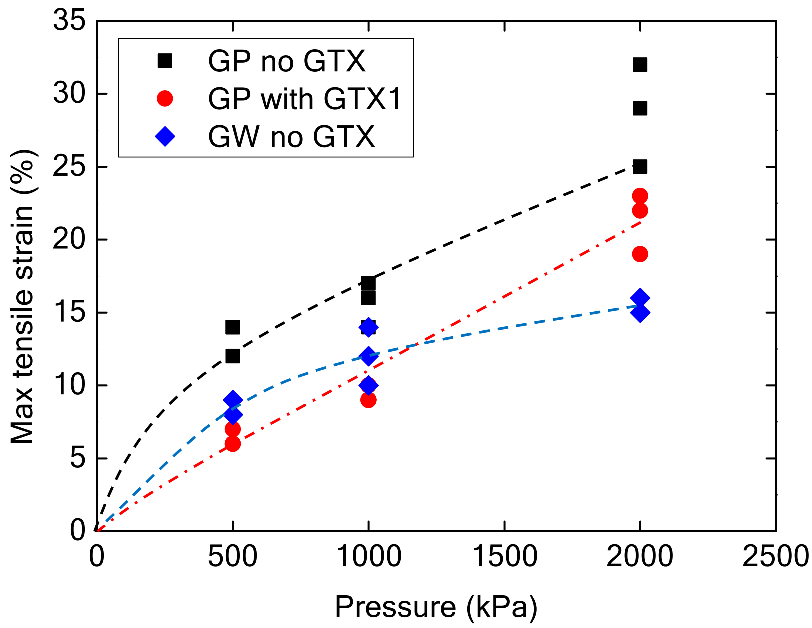

Fig. 8. Three largest strains calculated from each test showing the effect of pressure, subgrade, and GTX protection layer

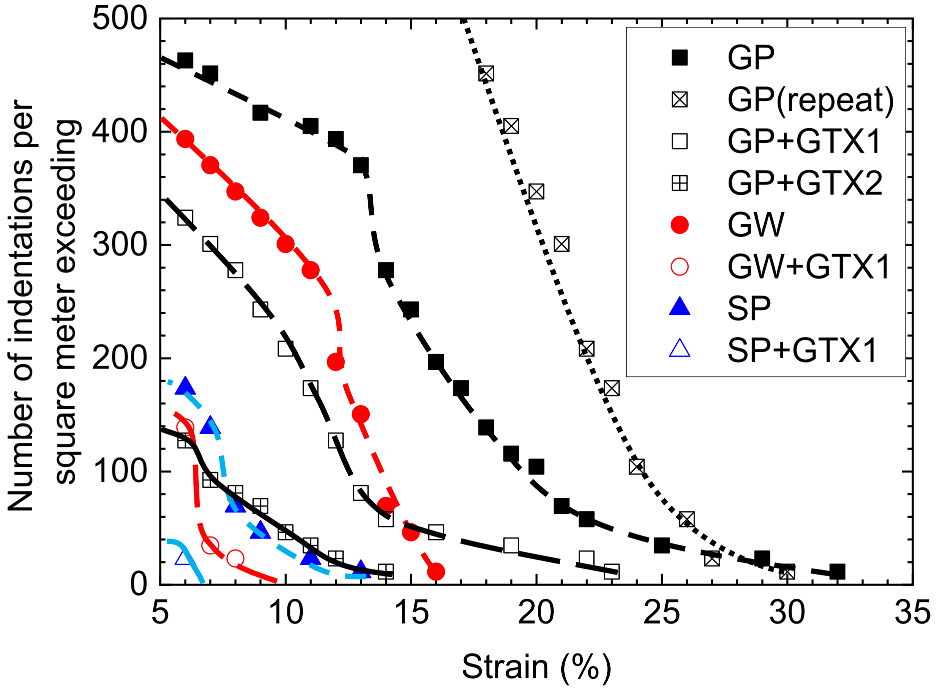

Fig. 9. Distributions of GMB tensile strains ≥ 5% per square meter GMB with subgrades of GP, GW, and SP at 2000 kPa